Express Polymer Letters Vol.19, No.2 (2025) 192–200
Available online at www.expresspolymlett.com
https://doi.org/10.3144/expresspolymlett.2025.14

Research article

Linear Drucker-Prager yield criterion calibration for polypropylene under multiaxial load

Adam Kasprzak[1,2*]

[1]Department of Machine Design and Research, Wrocław University of Science and Technology, Łukasiewicza 7/9, 50-371 Wrocław, Poland
[2]Robert Bosch Sp. z o. o., Wrocławska 43, 55-095 Mirków, Poland

Received 14 August 2024; accepted in revised form 17 November 2024

Abstract. This study focuses on calibrating the linear Drucker-Prager yield criterion for polypropylene under multiaxial loading conditions, using the Arcana fixture to achieve a wide range of triaxiality states. The Drucker-Prager criterion has been adapted for polymers, composites, and metals due to its ability to reflect the influence of hydrostatic pressure on yield stress. This study employs the Arcana fixture, which allows for testing flat plate samples under various angles, thereby simulating different stress states from pure shear to biaxial tension. Additionally, uniaxial compression tests were conducted to extend the range of triaxiality. The material used in this study is Sabic 83MF10, a polypropylene polymer. Samples were prepared by injection moulding and cut to specific dimensions. Tests were performed using a universal testing machine with the Arcana fixture, and the results were analysed to determine the yield strength, pressure, and triaxiality for each sample. The results showed a linear relationship between von Mises stress and hydrostatic pressure, with a friction angle (β) of 20.65° and material cohesion (*d*) of 27.81. The numerical simulations in Abaqus confirmed the validity of the Drucker-Prager model, accurately reflecting the moment of yielding for the tested samples.

Keywords: *finite element modelling, static testing, tensile testing, compressive testing, validation, Drucker-Prager*

1. Introduction

The introduction of polymeric materials to the market, specifically polypropylene in 1951 [1], represented a pivotal advancement in the field of materials science and engineering. These polymers have since become integral across a diverse array of industrial applications, such as automotive, medical, construction, electronics and consumer goods [2–4]. The preference for polymeric materials, particularly polypropylene, is based on their outstanding mechanical properties, intrinsic resistance to ageing, capability to maintain dimensional stability throughout their lifecycle, superior resistance to crack initiation or propagation, and their suitability for high-volume manufacturing processes such as extrusion and injection moulding [5–7].

Effective process of designing and validating components made of polymers in industries requires the usage of simulation, including the Finite Element Method [8]. To make this possible, it is necessary to accurately represent the behaviour of plastics under the different loading regimes and to reflect them in the numerical material model [9–11]. In addition to the commonly known nonlinear behaviour of thermoplastics, the influence of strain rate, temperature, stress state and loading type [12–15], the critical phenomena is the influence of the hydrostatic pressure on the yield stress, plastic flow and the destruction criterion [16–18]. Studies conducted in the past have clearly demonstrated the occurrence of different elastoplastic properties for loads of different

*Corresponding author, e-mail: adam.kasprzak@pwr.edu.pl

characteristics resulting from tests ranging from compression, through shear, to tension [19–22].

One of the widely used constitutive models capable of reproducing plastic behaviour is the linear Drucker-Prager criterion, which makes the transition of the material to the plastic range, *i.e.* the value of the yield stress, dependent on the value of the hydrostatic pressure. Thanks to this, it is possible to distinguish the behaviour of polymers under different load conditions, including the fact that for most thermoplastics, the yield strength for compression is higher than for tension [23–26]. The method originally came from soil research, but it has found wide application for plastics, composites and metals [27–30].

This article focuses on the usage of the Arcana fixture, which is widely used when the only possible form of material samples are flat plates with a defined thickness [31–36]. Most mentioned papers focused on the metal parts, for which it's feasible to produce the undercuts from both sides (for the tension tests) or on the 3D printed polymers, for which it's possible to produce axisymmetric samples (for the compression tests). It is necessary to properly cut the plates to obtain a multiaxial state of tension using an appropriate fillet radius at the necking point. An additional verification is a uniaxial compression test, which extends criteria to the compression state. The obtained material model is finally tested in the Abaqus numerical software to confirm the compliance of the obtained parameters for the Drucker-Prager model and the numerical simulations carried out using it with the real behaviour of polypropylene samples.

2. Material behavior

The stress tensor ($\boldsymbol{\sigma_{ij}}$) according to the matrix form from Equation (1), can be explained using the hydrostatic (mean) stress tensor ($\boldsymbol{\sigma_h}$), which is responsible for the volumetric change and the deviatoric stress tensor ($\mathbf{s_{ij}}$), which cause the body shape deviation:

$$\boldsymbol{\sigma_{ij}} = \begin{pmatrix} \sigma_{xx} & \sigma_{xy} & \sigma_{xz} \\ \tau_{yx} & \sigma_{yy} & \tau_{yz} \\ \tau_{zx} & \tau_{zy} & \sigma_{zz} \end{pmatrix} = \begin{pmatrix} \boldsymbol{\sigma_h} & 0 & 0 \\ 0 & \boldsymbol{\sigma_h} & 0 \\ 0 & 0 & \boldsymbol{\sigma_h} \end{pmatrix} + \begin{pmatrix} s_{xx} & s_{xy} & s_{xz} \\ s_{yx} & s_{yy} & s_{yz} \\ s_{zx} & s_{zy} & s_{zz} \end{pmatrix} = \boldsymbol{\sigma_h}\delta_{ij} + \mathbf{s_{ij}} \tag{1}$$

where the Kronecker Delta function is defined by Equation (2):

$$\delta_{ij} = \begin{cases} 1, & if \quad i = j \\ 0, & if \quad i \neq j \end{cases} \tag{2}$$

The dilatation state defined by the pressure ($\mathbf{p}$) could be drawn using the first invariant of the stress tensor ($\mathbf{I_1}$) (Equation (3)):

$$\mathbf{p} = -\sigma_{\mathbf{h}} = -\frac{1}{3} trace(\sigma_{ij}) = -\frac{\sigma_{xx} + \sigma_{yy} + \sigma_{zz}}{3} = -\frac{\mathbf{I_1}}{3} \tag{3}$$

Equivalent stress called von Mises (q) is defined by second invariant of deviator state (J_2) (Equation (4) and (5)):

$$q = \sigma_{eq} = \sqrt{3J_2} \tag{4}$$

$$J_2 = \frac{(\sigma_{xx} - \sigma_{yy})^2 + (\sigma_{yy} - \sigma_{zz})^2 + (\sigma_{zz} - \sigma_{xx})^2}{6} + \tau_{xy} + \tau_{yz} + \tau_{yz} \tag{5}$$

Thee thirst invariant of deviator state (J_3) needed to explain the Drucker-Prager criterion could by defined by Equations (6) and (7):

$$r = J_3 = \det(s_{ij}) \tag{6}$$

$$\det(s_{ij}) = \sigma_{xx}\sigma_{yy}\sigma_{zz} + \tau_{xy}\tau_{yz}\tau_{zx} + \tau_{xz}\tau_{yx}\tau_{zy} - \tau_{xz}\sigma_{yy}\tau_{zx} - \tau_{xy}\tau_{yx}\sigma_{zz} - \sigma_{xx}\tau_{yz}\tau_{zy} \tag{7}$$

The linear Drucker–Prager criterion commonly used for polymers can be represented in the meridian plane by the yield surface using the deviatoric stress factor (t) as a function of the hydrostatic pressure (p) as in the Figure 1, where the parameters defining its location are the friction angle (β) and the material cohesion (d) according to the Equation (8):

$$t = d + \tan\beta \tag{8}$$

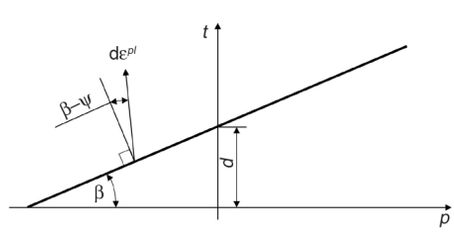

Figure 1. Yield surface and flow direction for linear Drucker-Prager model.

where the deviatoric stress factor (t) could be defined by Equation (9):

$$t = \frac{1}{2}q\left[1 + \frac{1}{\mathbf{K}} - \left(1 - \frac{1}{\mathbf{K}}\right)\left(\frac{r}{q}\right)^3\right] \tag{9}$$

using the ratio of the yield stress for triaxial tension and compression (**K**), which could be described on the deviatoric plane in Figure 2. Based on the research on polypropylene [22] and due to the limited scope of possible tests on the Arcana fixture, a **K** factor of 1 was assumed. Due to this $t = q$ on Figure 1. The plastic flow direction ($d\varepsilon^{pl}$) for polymer could be defined in Equation (10) by the dilatation angle (ψ) using the Poison ratio (ν) [37, 38]:

$$\psi = \tan^{-1}\left[\frac{3(1-2\nu)}{2(1+\nu)}\right] \tag{10}$$

In Equation(8):

- tangent of the friction angle (β) represents the sensitivity for the hydrostatic pressure (p),
- the material cohesion (d) reflects the isotropic hardening, which could be defined by Equation (11) using uniaxial tension (σ_t), compression (σ_c) or shear (τ) yield stress:

$$d = \left(\frac{1}{\mathbf{K}} + \frac{1}{3}\tan\beta\right)\sigma_t = \left(1 - \frac{1}{3}\tan\beta\right)\sigma_c = \\ = \frac{\sqrt{3}}{2}\left(1 + \frac{1}{\mathbf{K}}\right)\tau \tag{11}$$

The Drucker-Prager yield surface in the reverse principal axes is a cone around the hydrostatic axis with a circular cross-section for the **K** factor equal to 1, as in Figure 3.

To clearly determine the loading state of the material, the triaxiality (η) parameter (Equation (12)) should be used, the basic values of which are given in Table 1.

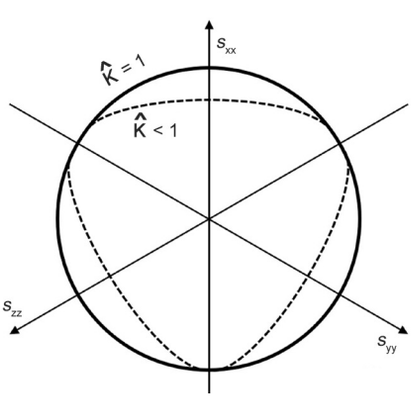

Figure 2. Yield surfaces for different ratios of the yield stress for triaxial tension and compression (**K**) on the deviatoric plane.

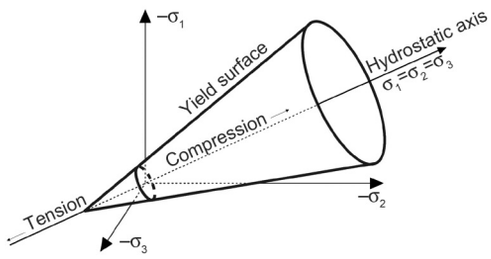

Figure 3. Yield surfaces in the reverse principal axes for the linear Drucker-Prager criterion.

Table 1. Example of the triaxiality values for different stress states.

Stress state	Triaxiality (η)
Triaxial tension	∞
Biaxial tension	2/3
Uniaxial tension	1/3
Shear	0
Uniaxial compression	–1/3
Biaxial compression	–2/3
Triaxial compression	–∞

$$\eta = \frac{p}{q} \tag{12}$$

3. Material, samples and experimental techniques

The following tests were performed for the thermoplastic Sabic 83MF10 material, universal polypropylene polymer provided by the Saudi Basic Industries Corporation (SABIC) and the basic parameters of which are presented in Table 2. The dilatation angle was calculated based on Equation (2).

Due to the fact that despite the lack of reinforcing inclusions in the material, such as fibres, noticeable anisotropy of properties is possible [41, 42], it was decided to cut samples from the plate far away from the injection points. This allowed us to obtain a quasi-random arrangement of molecules.

The tension and shear samples subjected to the analysis on a Zwick-type universal testing machine with the Arcana fixture were obtained in the form of flat plates received in the injection moulding process, with a thickness of 2.2 mm. The samples were

Table 2. Material data set for Sabic 83MF10.

Parameter	Value
Density	905 kg/m^3
Young modulus	1200 MPa
Poisson ratio	0.4
Dilatation angle	12.1°

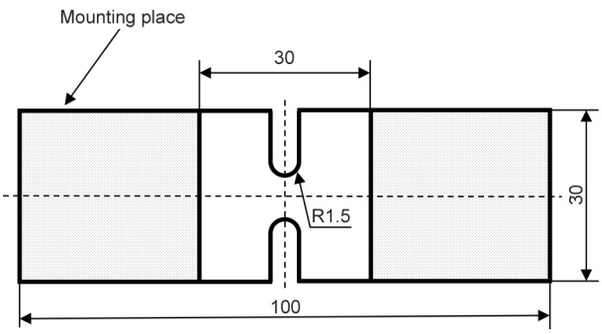

Figure 4. Sample scheme for tension and shear tests on arcana fixture.

machine cut with the radius of 1.5 mm and the dimensions described on Figure 4.

The sample for the uniaxial compression tests is a single cylinder with a diameter of 3 mm cut from the previously mentioned plates.

To achieve wide range of the triaxiality (η) and according to it different load type in stated between tension and shear, the Arcana fixture was used (Figure 5). This type of holder allows to stretch samples at angles from 0 to 90°. It consists of a pair of holders that secure it to the testing machine, two semicircular discs with holes that allow for mounting at 7.5° and holders that grip the tested sample directly. The entire structure is made of aluminium alloy 7075 (Fortal), ensuring high rigidity of the structure.

All tests on the Arcana fixture were performed with the constant head travel speed of 1 mm/s which allows to achieve strain rate ($\dot{\varepsilon}$) between 0.06 and 0.11/s during the tests. Due to the selected machine speed, it was possible to avoid, on the one hand, the influence of material hardening at the high strain rates described, *e.g.* by the Cowper-Symonds model [39, 40] and, on the other hand, the effect of the polymer relaxation [43, 44].

The universal testing machine used in the experiments was a Zwick Z100 equipped with a 500 N Zwick Xforce HP load cell, enabling simultaneous measurement of force and head travel. Due to the differences of several orders of magnitude in the Young's modulus for the metal elements included in the measuring system compared to the material from which the sample is made, it was not necessary to take into account the deformability of the remaining components. For each variant (Arcana tests and compression), three tests were performed, and two extreme cases (max and min values) in terms of yield strength were rejected from further evaluation due to numerical artefacts occurring in some measurements and limited material availability.

4. Experimental data processing and results

The linear Drucker-Prager criterion was chosen for further calibration due to the impossibility of obtaining the results for triaxial tension on flat samples with undercut. Figure 6 shows the results of tension (and shear) tests on the Arcana fixture and the result of the compression test of a cylindrical sample.

The following tests were performed to determine the yield strength, which, according to ISO 527-1, defines yielding as the first deviation in the true stress-strain curve from pure elastic response due to the lack of a distinct yield strength. Force (F) and displacement ($disp$) were measured using the Zwick embedded cross-head sensor. The values of triaxiality (η), pressure (p) and equivalent von Mises stress (q) were determined from FEM simulations representing the

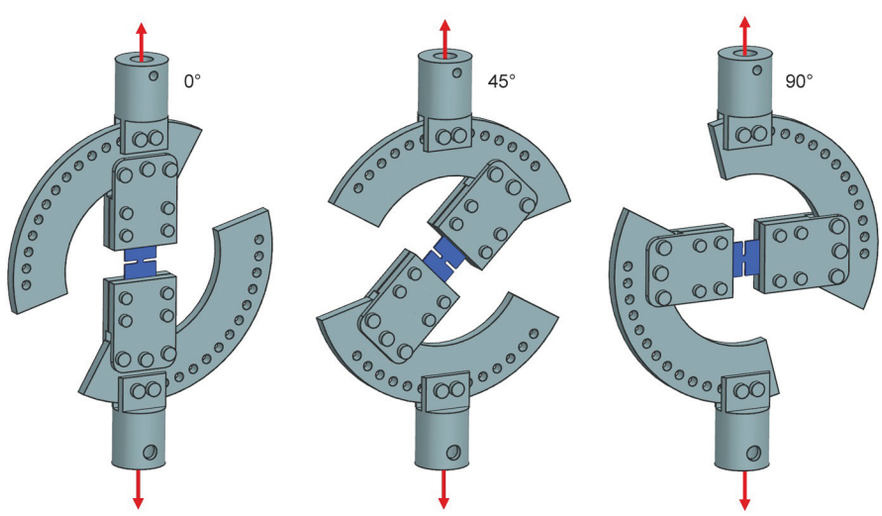

Figure 5. Arcana fixture for universal testing machine in different angle position.

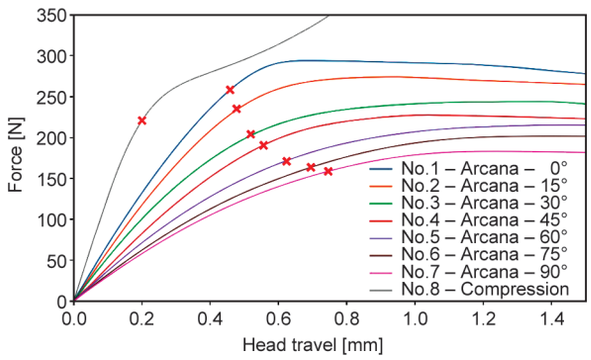

Figure 6. Force *vs.* head travel for Zwick from the Arcana or compression tests with the yield points.

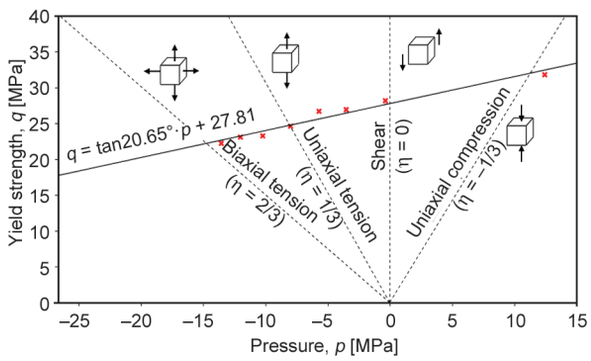

Figure 7. Linear Drucker-Prager yield von Mises stress as a function of pressure.

behaviour of the samples based on the calibration of the material curve with the load case as an average value for all of the elements included in cross-section in the critical most strained surface (the place with the lowest thickness). All results needed for further evaluation are described below in Table 3.

The larger the angle on the Arcana fixture, the lower the yield strength seems to be. This does not reflect the actual parameters due to the complex stress state, which is different for each sample. The decreasing apparent stiffness of the sample with the increasing angle results from the transition from pure tension to pure shear, where instead of the Young's modulus (E), the basic parameter defining elasticity is the Kirchhoff's (G) modulus, which calculated according to Equation (13) is 2.8 times lower:

$$G = \frac{E}{2(1+\nu)} \tag{13}$$

All the results mentioned in Table 3 were described as a linear function of Drucker-Prager yield criteria in Figure 7. The regression line was obtained using a solver, which has the objective function with scope to minimise the R^2 error value.

Table 3. Material data set for Sabic 83MF10.

Sample	Yield strength, q [MPa]	Pressure, p [MPa]	Triaxiality, η [–]
No 1 – Arcana – 0°	22.24	–13.57	0.61
No 2 – Arcana – 15°	23.12	–12.03	0.52
No 3 – Arcana – 30°	23.29	–10.24	0.44
No 4 – Arcana – 45°	24.64	–8.01	0.33
No 5 – Arcana – 60°	26.72	–5.72	0.21
No 6 – Arcana – 75°	26.96	–3.54	0.13
No 7 – Arcana – 90°	28.21	–0.39	0.01
No 8 – compression	31.83	12.41	–0.39

Table 4. Drucker-Prager linear model for Polypropylene Sabic 83MF10.

Parameter	Value
β	20.65°
d	27.81

As can be seen in the above graph, the results obtained for the Arcana fixture correspond to the values from pure shear (η = 0) to biaxial tension (η = 2/3), which was possible thanks to the proposed undercuts on flat samples. The disc compressed on the strength machine obtained a result slightly lower (η < –1/3) than for uniaxial compression due to its relatively small thickness and the friction occurring in the test between the upper and lower external surfaces of the sample and the contact linings of the testing machine. The final values for the linear Drucker-Prager criteria are described in Table 4.

All points achieved an average R^2 error value of 0.35, which suggests a very good fit to the linear relationship. An extension of the proposed linear criterion can be the tension cut-off, which determines the limiting value of the tensile pressure (p_t), beyond which the plastic deformation occurs, regardless of the value of von Mises stress (q) [45].

5. Material model validation using FEM simulation

In order to confirm the correct validation of the Drucker-Prager model, the simulations were performed on the previously tested samples and the calculation results in Abaqus were compared to the values obtained on the strength test bench. The implicit simulations were used using the Abaqus Standard solver. The discretised models used in the simulations (shown in Figure 8) for the Arcana and

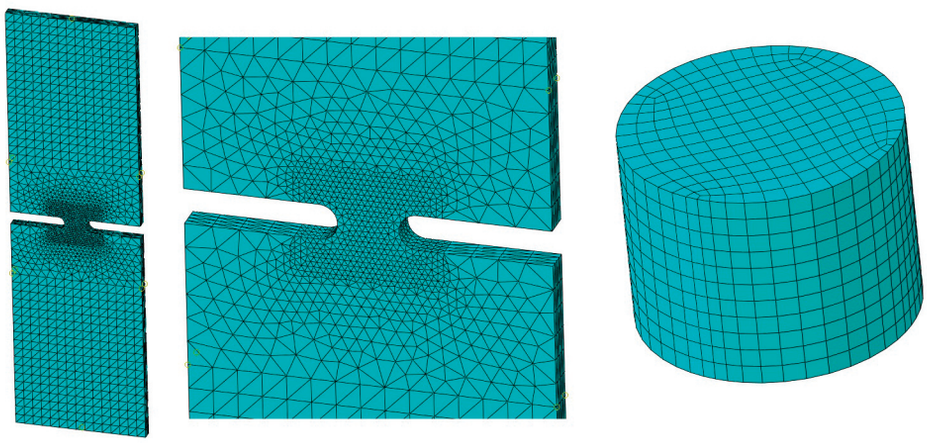

Figure 8. Numerical models overview for Arcana tension and compression tests.

compression have respectively 16263 C3D10, the 10-node quadratic tetrahedron elements with characteristic size of 0.5 mm in the critical space and 2200 C3D20, 20-node quadratic hexahedral elements with 0.2 mm for the whole geometry.

The finite element simulation was performed in a way that was designed to reproduce the actual test conditions as precisely as possible. For the samples tested on the Arcana fixture, the model was completely fixed on the lower side in the locations indicated as mounting place (35 mm from each end) in Figure 4. On the other side, a displacement was imposed in the vertical direction using kinematic coupling in Abaqus software. The Arcana fixture itself was not included in the simulation due to the stiffness of the entire structure made of aluminium that was several orders of magnitude higher, due to this to simulate each angle set-up in Arcana fixture tests it was required to translate displacement direction by dedicated angle according to vverticalaxis from 0 to 90°. For the disc compressed on both sides, the contact surfaces were simulated with a friction coefficient of 0.2, of which only one, the upper surface, moves towards the lower fixed plane. In order to follow the simulation progress above the yield point, the yield curve shown in Figure 9 was determined using the numerical calibration from the sample no 1 (Arcana – 0°) test curve.

The hardening behaviour was determined to range from 0 to 0.4 of the plastic strain and implemented in the Abaqus numerical software in tabular form with 17 points. Based on the above data, a comparison (in Figure 10) between the previous laboratory results and the numerical simulation results was made for all proposed samples.

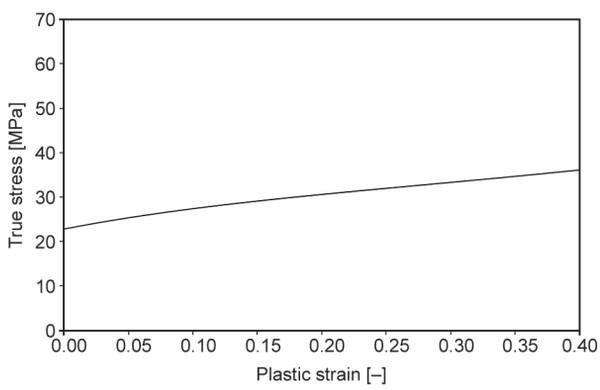

Figure 9. Hardening behaviour (plasticity curve) for numerical calculation calibrated from sample no 1 (Arcana – 0°).

As shown in the above graph, the simulation result shows the moment of yielding with a satisfactory result. The moment of appearance of the first plasticised finite elements and the transition of the entire critical cross-section into the plastic range are clearly visible. Due to the determination of the plasticity curve used for simulation based on sample no. 1, the

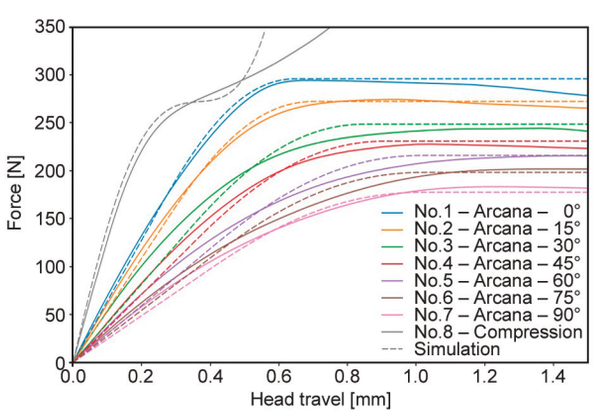

Figure 10. Force *vs.* head travel comparison between laboratory Zwick from Arcana or compression tests and numerical simulation results.

simulation course outside the elastic range is best shown. For models with an angle of setting above 30°, the laboratory results are characterised by a less clear moment of yielding compared to the simulation results. This may result from the settings in the Abaqus program, which do not take into account the possibility of the small angular movements of the samples at the place of attachment, which can occur during tests on the Arcana fixture. For the compressed sample, the moment of yielding is shown satisfactorily in the numerical model. However, a comparison of the course in the plastic range shows clearly that the yield curve differs significantly from that obtained from the tensile sample. The anisotropic nature of the elastic range is noticeable, which is demonstrated by the fact that for Arcana fixture settings close to 90° introducing a shear state in the sample, the Young Modulus (E) values are nearly 10% lower than those originally used in the simulation.

6. Conclusions and areas for further research

The comprehensive study of the Drucker-Prager presented in this article has shown a noticeable and significant linear dependence of the yield strength on the material state and, consequently, an unequivocal effect of the pressure on the criterion under study. The proposed approach using a specially manufactured Arcana fixture with samples with the special undercuts allows for the representation of the state from pure shear to biaxial tension, which is not possible using standard samples. The supplementation and extension of the studies to the scope of uniaxial compression is a compression test performed on a slender disc. The obtained results uniformly achieve a linear character of variation.

All previously laboratory-tested samples were numerically simulated, which allowed us to confirm the ability of the Drucker-Prager criterion implemented in the Abaqus program to properly reflect the moment of plasticisation of samples. Due to the demonstrated variable course of the plasticisation curve for different material loading states (Triaxiality), it seems advisable to take this phenomenon into account in future studies. At the moment, there are no ready-made solutions. Due to the stiffening of the numerical model of the sample mounting points in the fixture, a small deviation occurred for the elastic range in samples with a machine inclination angle >15°.

Further research should focus on the longer range of triaxiality, above 2-axis stretching, and determine the so-called tension cut-off, which defines the pressure at which the material immediately plasticises. A certain simplification of this phenomenon may be an attempt to calibrate the exponent or hyperbolic model, which indirectly takes into account the mentioned phenomenon. An additional benefit would be to conduct tests on an increased number of samples.

Acknowledgements

The article was created as part of the 6th edition of the program of the Minister of Education and Science entitled 'Implementation doctorate' Agreement No. DWD/6/0399/2022.

References

[1] Stinson S.: Discoverers of polypropylene share prize. Chemical and Engineering News, **65**, 30 (1987). https://doi.org/10.1021/cen-v065n010.p030

[2] Fried J. R.: Polymer science and technology. Prentice Hall, Upper Saddle River (2014).

[3] Young R. J., Lovell P. A.: Introduction to polymers. CRC Press, Boca Raton (2011). https://doi.org/10.1201/9781439894156

[4] Vasile C., Pascu M.: Practical guide to polyethylene. Rapra, Telford (2005).

[5] Maddah H. A.: Polypropylene as a promising plastic: A review. American Journal of Polymer Science, **6**, 1–11 (2016). https://doi.org/10.5923/j.ajps.20160601.01

[6] Hossain M. T., Shahid M. A., Mahmud N., Habib A., Rana M. M., Khan S. A., Hossain M. D.: Research and application of polypropylene: A review. Nano, **19**, 2 (2024). https://doi.org/10.1186/s11671-023-03952-z

[7] Karger-Kocsis J., Bárány T.: Polypropylene handbook. Springer, Berlin (2019). https://doi.org/10.1007/978-3-030-12903-3

[8] Maier C., Calafut T.: Applications. in 'Polypropylene' (eds.: Maier C., Calafut T.) William Andrew, Norwich, 87–107 (1998).

[9] Johri N., Agarwal G., Mishra R. K., Thakur H. C.: FEM analysis of polymeric hybrid composites. Materials Today: Proceedings, **57**, 383–390 (2022). https://doi.org/10.1016/j.matpr.2021.12.248

[10] Du S., Hamdi M., Sue H-J.: Experimental and FEM analysis of mar behavior on amorphous polymers. Wear, **444–445**, 203155 (2020). https://doi.org/10.1016/j.wear.2019.203155

[11] Gariya N., Prasad B., Kumar P.: FEM based analysis of soft polymer composites with crack. Materials Today: Proceedings, **28**, 2426–2430 (2020). https://doi.org/10.1016/j.matpr.2020.04.720

[12] Ayoub G., Zaïri F., Naït-Abdelaziz M., Gloaguen J. M.: Modelling large deformation behaviour under loading–unloading of semicrystalline polymers: Application to a high density polyethylene. International Journal of Plasticity, **26**, 329–347 (2010). https://doi.org/10.1016/j.ijplas.2009.07.005

[13] Laiarinandrasana L., Besson J., Lafarge M., Hochstetter G.: Temperature dependent mechanical behaviour of PVDF: Experiments and numerical modelling. International Journal of Plasticity, **25**, 1301–1324 (2009). https://doi.org/10.1016/j.ijplas.2008.09.008

[14] Arruda E. M., Boyce M. C., Jayachandran R.: Effects of strain rate, temperature and thermomechanical coupling on the finite strain deformation of glassy polymers. Mechanics of Materials, **19**, 193–212 (1995). https://doi.org/10.1016/0167-6636(94)00034-E

[15] Chou S. C., Robertson K. D., Rainey J. H.: The effect of strain rate and heat developed during deformation on the stress-strain curve of plastics. Experimental Mechanics, **13**, 422–432 (1973). https://doi.org/10.1007/BF02324886

[16] Alves M., Jones N.: Influence of hydrostatic stress on failure of axisymmetric notched specimens. Journal of the Mechanics and Physics of Solids, **47**, 643–667 (1999). https://doi.org/10.1016/S0022-5096(98)00060-X

[17] Abdul-Hameed H., Messager T., Ayoub G., Zaïri F., Naït-Abdelaziz M., Qu Z., Zaïri F.: A two-phase hyperelastic-viscoplastic constitutive model for semi-crystalline polymers: Application to polyethylene materials with a variable range of crystal fractions. Journal of the Mechanical Behavior of Biomedical Materials, **37**, 323–332 (2014). https://doi.org/10.1016/j.jmbbm.2014.04.016

[18] Hong K., Strobl G.: Characterizing and modeling the tensile deformation of polyethylene: The temperature and crystallinity dependences. Polymer Science, Series A, **50**, 483–493 (2008). https://doi.org/10.1134/S0965545X08050027

[19] Hachour K., Zaïri F., Naït-Abdelaziz M., Gloaguen J. M., Aberkane M., Lefebvre J. M.: Experiments and modeling of high-crystalline polyethylene yielding under different stress states. International Journal of Plasticity, **54**, 1–18 (2014). https://doi.org/10.1016/j.ijplas.2013.06.004

[20] Rinaldi R., Gaertner R., Brunet M., Chazeau L., Vidal-Sallé E., Gauthier C.: Modeling of the mechanical behavior of amorphous glassy polymer based on the quasi-point defect theory – Part II: 3D formulation and finite element modeling of polycarbonate. International Journal of Non-Linear Mechanics, **46**, 507–518 (2011). https://doi.org/10.1016/j.ijnonlinmec.2010.12.006

[21] Olsson R.: A survey of test methods for multiaxial and out-of-plane strength of composite laminates. Composites Science and Technology, **71**, 773–783 (2011). https://doi.org/10.1016/j.compscitech.2011.01.022

[22] Manaia J. P., Pires F. A., de Jesus A. M. P.: Elastoplastic and fracture behaviour of semi-crystalline polymers under multiaxial stress states. Frattura ed Integrità Strutturale, **13**, 82–103 (2019). https://doi.org/10.3221/IGF-ESIS.47.08

[23] Pae K. D., Bhateja S. K.: The effects of hydrostatic pressure on the mechanical behavior of polymers. Journal of Macromolecular Science, Part C, **13**, 1–75 (1975). https://doi.org/10.1080/15321797508068145

[24] Olufsen S., Clausen A. H., Hopperstad O. S.: Influence of stress triaxiality and strain rate on stress-strain behaviour and dilation of mineral-filled PVC. Polymer Testing, **75**, 350–357 (2019). https://doi.org/10.1016/j.polymertesting.2019.02.018

[25] Christiansen A. W., Baer E., Radcliffe S. V.: The mechanical behaviour of polymers under high pressure. The Philosophical Magazine: A Journal of Theoretical Experimental and Applied Physics, **24**, 451–467 (1971). https://doi.org/10.1080/14786437108227400

[26] Ward I. M.: Review: The yield behaviour of polymers. Journal of Materials Science, **6**, 1397–1417 (1971). https://doi.org/10.1007/BF00549685

[27] Drucker D. C., Prager W.: Soil mechanics and plastic analysis or limit design. Quarterly of Applied Mathematics, **10**, 157–165 (1952). https://doi.org/10.1090/qam/48291

[28] Pulungan D., Lubineau G., Yudhanto A., Yaldiz R., Schijve W.: Identifying design parameters controlling damage behaviors of continuous fiber-reinforced thermoplastic composites using micromechanics as a virtual testing tool. International Journal of Solids and Structures, **117**, 177–190 (2017). https://doi.org/10.1016/j.ijsolstr.2017.03.026

[29] Naya F., González C., Lopes C. S., van der Veen S., Pons F.: Computational micromechanics of the transverse and shear behavior of unidirectional fiber reinforced polymers including environmental effects. Composites Part A: Applied Science and Manufacturing, **92**, 146–157 (2017). https://doi.org/10.1016/j.compositesa.2016.06.018

[30] Chen J., Wan L., Ismail Y., Hou P., Ye J., Yang D.: Micromechanical analysis of UD CFRP composite lamina under multiaxial loading with different loading paths. Composite Structures, **269**, 114024 (2021). https://doi.org/10.1016/j.compstruct.2021.114024

[31] Popelar C., Liechti K. A.: A distortion-modified free volume theory for nonlinear viscoelastic behavior. Mechanics of Time-Dependent Materials, **7**, 89–141 (2003). https://doi.org/10.1023/A:1025625430093

[32] Hao P., Ud Din I., Panier S.: Development of modified Arcan fixture for biaxial loading response of fiber-reinforced composites. Polymer Testing, **80**, 106148 (2019). https://doi.org/10.1016/j.polymertesting.2019.106148

[33] Cognard J. Y., Sohier L., Davies P.: A modified Arcan test to analyze the behavior of composites and their assemblies under out-of-plane loadings. Composites Part A: Applied Science and Manufacturing, **42**, 111–121 (2011). https://doi.org/10.1016/j.compositesa.2010.10.012

[34] Hung S. C., Liechti K. M.: An evaluation of the Arcan specimen for determining the shear moduli of fiber-reinforced composites. Experimental Mechanics, **37**, 460–468 (1997). https://doi.org/10.1007/BF02317314

[35] Arcan M., Hashin Z., Voloshin A.: A method to produce uniform plane-stress states with applications to fiber-reinforced materials. Experimental Mechanics, **18**, 141–146 (1978). https://doi.org/10.1007/BF02324146

[36] Voloshin A., Arcan M.: Pure shear moduli of unidirectional fibre-reinforced materials (FRM). Fibre Science and Technology, **13**, 125–134 (1980). https://doi.org/10.1016/0015-0568(80)90041-X

[37] Morelle X. P., Chevalier J., Bailly C., Pardoen L., Lani F.: Mechanical characterization and modeling of the deformation and failure of the highly crosslinked RTM6 epoxy resin. Mechanics of Time-Dependent Materials, **21**, 419–454 (2017). https://doi.org/10.1007/s11043-016-9336-6

[38] Quino G., Gargiuli J., Pimenta S., Hamerton I., Robinson P., Trask R. S.: Experimental characterisation of the dilation angle of polymers. Polymer Testing, **125**, 108137 (2023). https://doi.org/10.1016/j.polymertesting.2023.108137

[39] Xu M-M., Huang G-Y., Feng S-S., McShane G. J., Stronge W. J.: Static and dynamic properties of semicrystalline polyethylene. Polymers, **8**, 77 (2016). https://doi.org/10.3390/polym8040077

[40] Marangoni A. L., Massaroppi E.: Cowper-symonds parameters estimation for ABS material using design of experiments with finite element simulation. Polímeros, **27**, 220–224 (2017). https://doi.org/10.1590/0104-1428.04016

[41] Schrauwen B. A. G., van Breemen L. C. A., Spoelstra A. B., Govaert L. E., Peters G. W. M., Meijer H. E. H.: Structure, deformation, and failure of flow-oriented semicrystalline polymers. Macromolecules, **37**, 8618–8633 (2004). https://doi.org/10.1021/ma048884k

[42] Katti S. S., Schultz M.: The microstructure of injection-molded semicrystalline polymers: A review. Polymer Engineering and Science, **22**, 1001–1017 (1982). https://doi.org/10.1002/pen.760221602

[43] Swallowe G. M.: Relaxations in polymers. in 'Mechanical properties and testing of polymers' (ed.: Swallowe G. M.) Polymer Science and Technology Series, Vol. 3, Springer, Dordrecht, **42**, 195–198 (1999). https://doi.org/10.1007/978-94-015-9231-4_42

[44] Jourdan C., Cavaille J. Y., Perez J.: Mechanical relaxations in polypropylene: A new experimental and theoretical approach. Journal of Polymer Science Part B: Polymer Physics, **27**, 2171–2184 (1989). https://doi.org/10.1002/polb.1989.090271115

[45] Krabbenhoft K., Karim M. R., Lyamin A. V., Sloan S. W.: Associated computational plasticity schemes for nonassociated frictional materials. International Journal for Numerical Methods in Engineering, **90**, 1089–1117 (2012). https://doi.org/10.1002/nme.3358